Rheol Acta (2004) 43: 210–222
DOI 10.1007/s00397-003-0333-8

ORIGINAL CONTRIBUTION

Nicolas Devaux
Bernard Monasse
Jean-Marc Haudin
Paula Moldenaers
Jan Vermant

Rheooptical study of the early stages of flow enhanced crystallization in isotactic polypropylene

Received: 1 July 2003
Accepted: 22 September 2003
Published online: 16 January 2004

Electronic supplementary material to this paper can be obtained by using the Springer Link server located at http://dx.doi.org/10.1007/s00397-003-0333-8

N. Devaux · B. Monasse · J.-M. Haudin
Centre de Mise en Forme des Matériaux,
Ecole des Mines de Paris,
UMR C.N.R.S. 7635, B.P.207, F-06904
Sophia-Antipolis, France

P. Moldenaers · J. Vermant (✉)
Department of Chemical Engineering,
K.U. Leuven, W. de Croylaan 46,
B-3001 Leuven, Belgium
E-mail: jan.vermant@cit.kuleuven.ac.be

Present address: N. Devaux
Cerdato, ATOFINA, F-27470 Serquigny,
France

Abstract The effect of a shear flow on the early stages and the kinetics of isothermal crystallization of an isotactic polypropylene has been studied experimentally. In the shear rate region where crystallization proceeds through point-like precursors, the magnitude of the shear rate, the shearing time as well as the instant in time at which the deformation starts have all been varied, in combination with rheooptical measurements. These include depolarized light intensity and birefringence. In agreement with previous work, above a critical shear rate and a critical shearing time, the crystallization kinetics are enhanced. Somewhat surprisingly, below a characteristic time, $t_{0,max}$, the kinetics are not affected by the instant in time at which flow is applied or stops. As long as flow takes place before this critical dwell time, only the shearing time and primarily the magnitude of the shear rate seem to matter. When flow is started only after $t_{0,max}$, its effect to accelerate crystallization kinetics becomes less efficient. The range over which the different parameters have an effect have been compared to the rheological relaxation times and to the measurements of global chain extension. To investigate the effects of flow on the early stages in more detail, time resolved Small-Angle Light Scattering experiments were used to detect changes in the density and orientation fluctuations. Measurements explicitly compare the effect of temperature and shear flow on the kinetics and the intensity of the density fluctuations.

Keywords Flow enhanced crystallization · Rheooptics · Light scattering · Polymer crystallization

Introduction

During processing, molten polymers are unavoidably subjected to strong deformations and complex thermal histories. Semicrystalline materials will crystallize after or even during flow. The properties of the final product will hence be affected by both the thermal and the mechanical history that the polymer experiences in the molten state. To improve our understanding of the crystallization process from a fundamental point of view, it has proven useful to separate the thermal and flow effects. Several researchers have studied flow enhanced crystallization in well defined flows and under isothermal conditions. The focus of previous work in the literature has mainly been on overall kinetics (Lagasse and Maxwell 1976; Andersen and Carr 1978; Tribout et al. 1996) and the changes in the induction times (Lagasse and Maxwell 1976; Sherwood et al. 1977). It has been shown that both factors are considerably enhanced by flow, the main effect of flow being on nucleation density. Under certain conditions, however, even the morphologies will change as a consequence of the deformation, from the typical spherulite encountered under quiescent conditions to oriented crystalline

structures, such as shish-kebab or row-nucleated structures (Keller and Machin 1967). Additionally, it has been shown that flow can also affect crystal growth kinetics (Monasse 1995; Tribout et al. 1996).

Static polymer crystallization from the molten state is known to proceed through a mechanism of nucleation, mainly heterogeneous, and growth (Wunderlich 1980). For heterogeneous crystallization of polymers from the molten state, the classical theory has been described by Binsbergen (1973), in which the nucleation is modeled as a step mechanism of deposit of polymer segments onto a substrate resulting in the formation of a nucleus. When the size of this nucleus exceeds a critical size, the growth of the crystalline phase becomes energetically favorable. However, measurements of such critical nucleus have only been possible for the case of phase separating polymer blends (Lefebvre et al. 1999); for polymer crystallization the critical nuclei have not yet been measured. Small-Angle X-ray Scattering (SAXS) and Wide-Angle X-ray Diffraction (WAXD) even seem to reveal a more complex behavior. Terrill et al. (1998) suggest that it follows the Cahn-Hilliard theory for spinodal decomposition, although other researchers disagree on this point (see, e.g., Wang et al. 2000). Optical and light scattering techniques have also been used to study the evolution of the early stages of crystallization. Okada et al. (1992) used Small-Angle Light Scattering (SALS) using polypropylene samples. The analysis of scattering patterns showed that large scale density fluctuations develop and subsequently relax before a crystalline structure appears. Pogodina et al. (1999) extended their work, and combined the SALS experiments with rheological measurements. Based on the evolution of the linear viscoelastic moduli with time and frequency, they suggested that during the early stages of crystallization a gel-like structure develops, considerably before crystalline structures appear. Light scattering experiments gave correlation lengths of density fluctuations exceeding those from the SAXS studies by two orders of magnitude, i.e., 1 μm (Pogodina et al. 1999) as opposed to 100 Å (Terrill et al. 1998). Obviously, a clear picture of nucleation in the case of static crystallization is still lacking. The fact that nucleation is accompanied by larger scale fluctuations of the density will be exploited in the present work, as SALS experiments will be used to monitor their evolution.

Lagasse and Maxwell (1976) were the first to investigate the effects of shear flow on crystallization kinetics in a systematic manner. Using rheological measurements, they demonstrated that, beyond a critical shearing time, the induction times for viscosity increase were observed to decrease substantially. Janeschitz-Kriegl and coworkers (Liedauer et al. 1993; Jerschow and Janeschitz-Kriegl 1997) elaborated their work using optical measurements to find that the important parameters are shear rate and time of shearing.

The time for the birefringence to reach half its maximum value was found to be reduced by a factor containing the shear rate to the fourth power and the duration of shearing t_S squared, i.e., $\dot{\gamma}^{-4}t_s^{-2}$. It was later shown that this factor could change with differences in the molecular weight distributions and the addition of nucleating agents (Jerschow and Janeschitz-Kriegl 1997). It is not clear in which range of temperatures, shear rates and shearing times these scalings hold. Vleeshouwers and Meijer (1996) qualitatively confirmed this result that a short time shearing at high rate is the most effective, as deduced from the reduction of induction times measured by rheometry. Kumaraswamy et al. (1999) recently reported that, above a critical duration of shear time, the acceleration of crystallization kinetics saturates. Although effects of $\overline{M_w}$ and nucleating agents have been studied (Bashir et al. 1986; Duplay et al. 1999; Jerschow and Janeschitz-Kriegl 1997), it is still not fully understood what exactly controls the dependencies on shear rate and shearing time.

Shear flow affects nucleation kinetics tremendously, and has received much attention (Liedauer et al. 1993; Monasse 1995; Vleeshouwers and Meijer 1996; Jerschow and Janeschitz-Kriegl 1997; Kumaraswamy et al. 1999; Duplay et al. 2000; Pogodina et al. 2001; Kumaraswamy et al. 2002). Several explanations have been proposed. Along the lines of the classical nucleation theories, the orientation and chain extension of the polymers can be expected to lower the entropy of the melt and hence lower the energy barrier for nucleation (McHugh 1982). Many models for flow enhanced crystallization are built on this principle (see, e.g., Coppola et al. 2001). Large scale, birefringent, threadlike precursors (see, e.g., Liedauer et al. 1993; Pogodina et al. 1999; Kumaraswamy et al. (1999) and flow-induced crystallization precursors have been observed (Kumaraswamy et al. 2002) and have been invoked as playing an important role in acceleration of the crystallization and the development of anisotropic crystalline morphologies. The mechanism by which these precursors develop and how they interfere with nucleation has not yet been clarified, but it has been shown that the pathway to nucleation can be altered by these intermediate structures (Kumaraswamy et al. 2002). Other researchers have suggested that a mere separation of the melt into more and less dense regions precedes nucleation (Terrill et al. 1998), a process which in turn could be affected by flow (McHugh and Spevacek 1991).

The objective of this paper is to study the effect of a well-defined shear flow history at moderate flow conditions on the phenomena observed during crystallization of a polypropylene sample. As the primary effect of flow is the enhancement of the nucleation, it is essential to understand how the early stages are affected by the application of a flow field. The short-time shearing protocol, introduced by Janeschitz-Kriegl and coworkers

(Liedauer et al. 1993), enables separation of flow, nucleation and growth phenomena. It has been used to study flow-enhanced crystallization under isothermal conditions at high shear rates (Jerschow and Janeschitz-Kriegl 1997; Liedauer et al. 1993; Kumaraswamy et al. 1999, 2002). In the present work, separation of flow, nucleation, and growth will be used as well, but using relatively high degrees of undercooling and moderate shear rates. Conditions will be such that only an increase of the number of point-like nuclei is observed, i.e., spherulitic morphologies will still be formed. It will be examined over which range of shearing times and shear rates the flow has an effect. The role of the different parameters will be compared to the relaxation times. The polymer orientation will be monitored using transient linear birefringence and compared to crystallization kinetics. Small-Angle Light Scattering measurements will be used to analyze the evolution of the spatial variations of density and orientation and how their kinetics and intensities are affected by the flow.

Experiments

Material and shearing devices Isotactic polypropylene (iPP) was chosen as the material under investigation, as it renders a comparison with literature data possible. A material with a rather high molecular weight $\left(\overline{M_w} = 338000, \text{ isotacticity } 94\%\right)$ and a wide distribution of macromolecular chain lengths $\left(I_p = \frac{\overline{M_w}}{\overline{M_n}} = 6.45\right)$ was selected, as strong effects of flow on crystallization can be anticipated for such materials (Duplay et al. 2000). Polymer pellets were supplied by AtoFina (France). Two devices were used to generate a controlled thermal and mechanical history: a modified Mettler FP52 hot stage equipped with sliding-plate (Monasse 1995) and a rotating plateplate flow cell (Linkam CSS, Linkam Scientific Instruments, UK). Both devices enable in situ optical measurements. The modified hot stage was used for optical microscopy experiments (including depolarized light intensity measurements) and the Linkam cell was mainly used for light scattering and flow birefringence. The observation zone in the Linkam cell is located at the middle of the radius of the upper plate ($r_0 = 7.5$mm from the center). Although the flow between rotating parallel plates is non-homogeneous, this is not a serious drawback as the observation zone is small and the local shear rate is constant and the strain can be varied at will. The sliding plate cell provides a homogeneous shear deformation, but only a limited strain can be applied. Hence, the two devices are complementary.

The shear rates that could be accessed with the Linkam CSS450 cell range from 0.1 to 2 s^{-1} . The lower limit was set by the relatively crude control of the motion of the top plate, inherent to the design of the device, which uses a stepper motor. At high shear rates and strains, shear fracture was observed. One factor complicated the calculation of the shear rate: significant deviations between the desired gap spacing, indicated by the instrument, and the real gap spacing were observed. Therefore, and this held true for experiments on both devices, the thickness of the sheared films was measured post-factum after crystallization and corrected for thermal expansion and density changes. Differences between the gaps indicated by the Linkam software and the post-factum measured thickness sometimes amounted to 50%.

Crystallization of iPP from the melt is highly temperature sensitive. Consequently, both shearing devices require accurate and absolute temperature calibration. Temperature in the modified hot stage is controlled by a Mettler FP52 module, and a supplementary constant nitrogen flux compensates for heat losses and reduces polymer oxidation. Calibration of the modified hot stage was performed by measuring the melting point of indium crystals at different heating rates (the onset of melting was detected by a drop in transmitted light intensity). Extrapolation to isothermal conditions leads to the equilibrium melting point of indium, which is known to be 156.6 °C. With this method the temperature can be calibrated to within 0.1 °C. It can be noted that the time to reach a desired temperature was less than 10 s in the temperature range explored. The Linkam CSS450 cell was also calibrated by this method. Additional measurements of temperature gradients in the different directions were performed using miniature platinum resistance thermometers (Pt100). The measurements showed that the Linkam CSS450 cell has a good temperature stability in time (≤ 0.2 °C) together with a fairly short equilibration time (< 30 s). Although temperature gradients were present, both in radial and normal directions, the temperature was found to be well-controllable at a fixed distance r_0 from the center of the plate.

Thermal and mechanical protocol The thermomechanical protocol used for the crystallization experiments is schematically depicted in Fig 1. The thermal protocol was essentially identical in all experi-

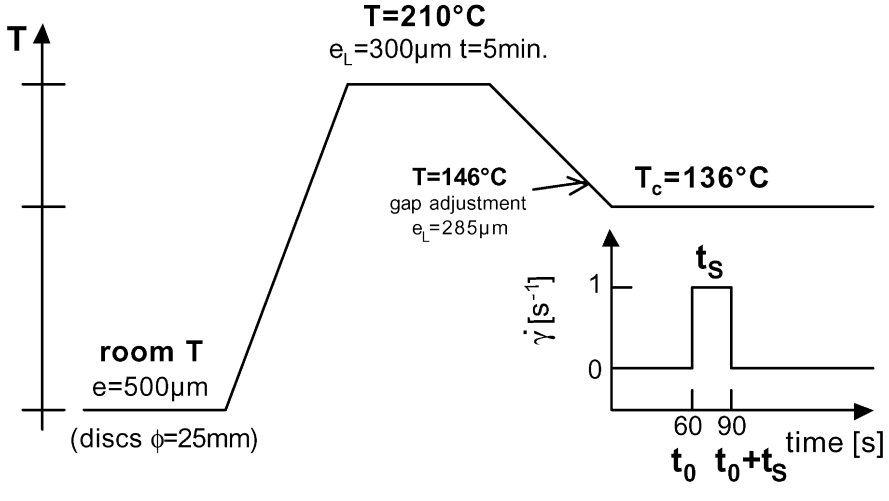

Fig. 1 Typical experiment with the thermal protocol and the flow history used for the polypropylene, $T_c = 136$ °C; example of typical shear flow conditions: $\dot{\gamma} = 1\ s^{-1}$, time after isothermal condition $t_0 = 60$ s, time of shearing $t_S = 30$ s

ments whereas the parameters in the mechanical protocol were varied systematically. Polymer films (thickness $\backsim 500$ μm) were prepared by pressing pellets at T = 210 °C for 5 min. Discs (ϕ = 25 mm) were subsequently cut out of these films. These discs were inserted into the Linkam and heated up to T_m = 210 °C. The gap was set to a value of approximately 300 μm by slowly lowering the upper glass plate of the Linkam. Subsequently, the sample was maintained at T_m for 5 min. Then the sample was cooled, at a fixed cooling rate of 10 °C/min, until the desired crystallization temperature, mostly 136 °C, was reached. During cooling, the gap was adjusted in order to compensate for the volumetric shrinkage of the sample that can cause the sample to detach from the plates, which interferes with the optical measurements. From the pVT measurements, the volumetric shrinkage is estimated to be 5% during cooling. The shrinkage occurring during crystallization is not accounted for. For the quiescent crystallization it was easily verified that the mild squeeze flow to adjust the gap does not affect the overall crystallization kinetics. The same thermomechanical protocol was used with the modified hot stage, except that a rectangular shape (40 mm×5 mm) was used and that the gap was not adjusted during cooling (gap is fixed by screws). Probably due to the compliance of this device, no problems of detachment were observed during crystallization.

Most of the isothermal experiments were performed at a temperature of 136 °C. This temperature corresponds to a mild degree of undercooling and to a regime III of growth in the classification of Lauritzen and Hoffman (1973) (see also, Monasse and Haudin 1985). DSC measurements and optical microscopy also showed that crystallization at this temperature under static conditions takes about 90 min and the radius of the spherulites reaches 50 μm before impingement (Devaux 2003).

In our experiments, two characteristic times are defined to describe the shear flow during isothermal crystallization (see Fig 1):

- t_0: the time elapsed between the instant at which the isothermal conditions are reached and the inception of the shear flow
- t_S: the duration of the shear flow at a fixed shear rate, $\dot{\gamma}$

A commonly used approach to evaluate the effect of shear flow is to start the flow immediately after isothermal conditions are reached ($t_0 = 0$). When experiments at different strains are compared, the moment at which flow is stopped will obviously vary. One specific aim of the present experiments is to verify whether there is an effect of the instant in time at which the flows are applied and stopped. As the structure is continuously evolving during crystallization, this cannot be ruled out a priori. Two experimental protocols were used for this investigation:

- Constant total strain, i.e., both shear rate and t_S are fixed, only t_0 is varied. This way, the same shear flow is applied at different instants. In this manner, the effect of orienting polymeric chains at different moments in time is investigated.
- Varying strain, while keeping the instant of flow cessation ($t_0 + t_S$) constant, the duration of shear flow (t_S) is varied. In this manner, the effect of varying the degree and duration of polymer chain orientation on crystallization are explored.

Rheooptical measurements The depolarized light intensity (DLI) was measured to monitor the overall kinetics under both static and flow conditions. For the sliding-plate device, the white light entering the objective (×20, n.a. = 0.4) of a polarizing microscope (Leica DMRX) is recorded with a photodiode that replaces one of the eyepieces of the microscope. The shearing cell is placed between crossed polarizers, the flow direction being parallel to the second polarizer. The light accumulated in the eyepiece contains the transmitted depolarized light as well as the light scattered by the spherulites, inside a cone angle $\theta = 22°$. Whereas a correction is necessary in the case of high nucleation rates (Ding and Spruiell 1996) the scattering contribution can be neglected in the case of low nucleation rates typical of isothermal crystallization. The ratio α between the transmitted intensity $I(t)$, corrected for the intensity prior to crystallization $I(0)$, to the maximum intensity observed at the end of crystallization I_∞, also corrected for $I(0)$, is defined as

$$\alpha(t) = \frac{I(t) - I(0)}{I_\infty - I(0)} \tag{1}$$

For the case of iPP, this ratio has been shown to be equal to the fraction of the volume occupied by the growing spherulites (Pratt and Hobbs 1976). Hence, although this is not a rigorous method valid for all types of polymers, the depolarized light intensity (DLI) and $\alpha(t)$ defined by Eq. (1) can be used here to monitor the overall kinetics of crystallization of iPP.

Flow birefringence can in principle be measured by monitoring the depolarized light intensity of a laser beam between crossed polarizers oriented at 45 and 135° with respect to the flow direction, but polarimetric techniques have a higher sensitivity and better time resolution. A rotary polarization modulation method, as suggested by Fuller and Mikkelsen (1989), was used here to measure the flow birefringence as a function of time.

A high modulation frequency makes it possible to study fast time-dependent phenomena. The orientation angle χ and the magnitude of the birefringence $\Delta n'$ can be determined simultaneously. The linear birefringence provides information on the distribution of the end-to-end vectors, i.e., the global chain extension (Fuller 1995).

Small Angle Light Scattering The optical train used for Small Angle Light Scattering experiments is presented in Fig 2. Light from a He-Ne laser passes successively through a Glan-Thomson polarizer (P), the sample contained in the Linkam CSS 450 flow cell, and a dichroic sheet analyzer (A). The scattering patterns are collected on a semitransparent screen. A rubber cylinder is used as

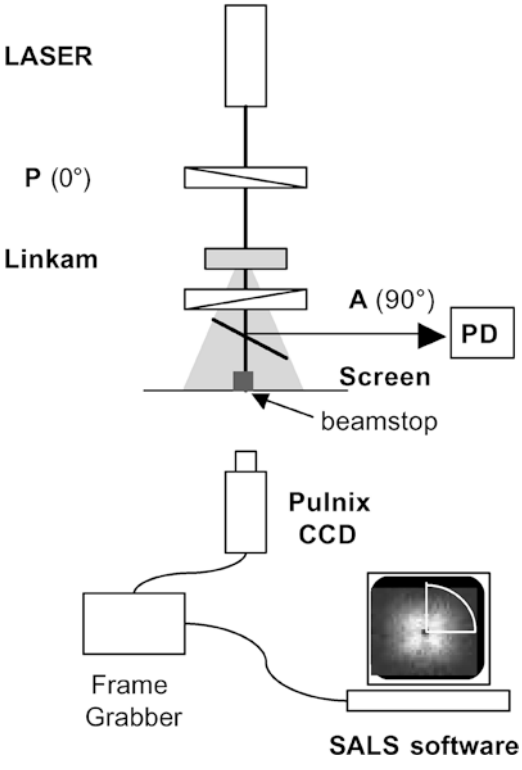

Fig. 2 Scheme of the setup for SALS experiments. Symbols are explained in the text

a beamstop. Because the nucleation phenomena involve weak signals, a high resolution (10 bits, 1300×1030 active pixels), light sensitive CCD progressive scan camera (Pulnix TM-1300) was used as the detector. To minimize noise during image processing, a digital frame grabber was used to transfer the images (TCI-digital from Coreco) to a PC. The homemade acquisition software allows for averaging of images to increase signal-to-noise ratios. The images were also corrected for thermal noise of the camera. The time interval between consecutive pictures can be as short as 100 ms. A home-developed software (SALSsoftware) enables integration over angular quadrants and determination of the anisotropy. Both polarized scattering experiments, with parallel polarizer and analyzer (V_V), and depolarized scattering experiments, with crossed polarizers (H_V), were performed. The depolarized H_V scattering patterns arise from variations in the anisotropic part of the dielectric tensor whereas the polarized V_V scattering patterns are due to variations in both the isotropic and anisotropic part. They can be analyzed by the statistical formalism of Stein and Wilson (1962). This approach assumes circularly symmetric scattering patterns. The fluctuations in the anisotropic part are attributed to spatial variations in orientation; the fluctuations in the isotropic part are due to spatial variations in the density. The scattered intensities are then given by (Stein and Wilson 1962)

$$I_{V_V} - \frac{4}{3} I_{H_V} \propto \langle \eta^2 \rangle \int_0^{+\infty} \gamma(r) \frac{\sin qr}{qr} 4\pi r^2 dr \tag{2}$$

$$I_{H_V} \propto \langle \delta^2 \rangle \int_0^{+\infty} f(r) \frac{\sin qr}{qr} 4\pi r^2 dr \tag{3}$$

where $\langle \eta^2 \rangle$ is the mean-square density fluctuation and $\gamma(r)$ its correlation function; $\langle \delta^2 \rangle$is the mean of the squared anisotropy and $f(r)$ is the correlation function of the orientation "fluctuations". The magnitude of the scattering vector is $|q| = (4\pi/\lambda) \sin(\theta/2)$, with θ being the polar scattering angle. As no a priori information is available on the nature of these correlation functions, it is more convenient to describe the evolution of the scattering patterns in terms of the invariants Q_η and Q_δ that represent respectively the importance of the spatial variations in density and orientation:

$$\begin{aligned} Q_\eta &= \int_0^{+\infty} \left(I_{V_V} - \tfrac{4}{3} I_{H_V}\right) q^2 \mathrm{d}q \propto \langle \eta^2 \rangle \\ Q_\delta &= \int_0^{+\infty} I_{H_V} q^2 \mathrm{d}q \propto \langle \delta^2 \rangle \end{aligned} \tag{4}$$

The bounds for integration were limited to [0.15 μm^{-1}] (lower bound corresponds to the beamstop) and integration was calculated on 90°angular quadrants. In most experiments, only the time scale of the evolution of the invariants was monitored, and they were normalized by their maximum values. In a limited number of experiments, the evolution of the absolute intensities was monitored. A non-polarizing beam splitter (see Fig 2) was placed after the analyzer at an angle of about 45° with respect to the incoming beam, and the reflected beam was sent through a pinhole into a sensitive photodiode (PD, Beaglehole Instruments, NZL). The intensity can be used to compare quantitatively between a reference case, static crystallization at 136 °C, and crystallization at different temperatures and after different shear flow histories.

Results

Rheological properties

The linear viscoelastic behavior of the iPP was investigated for two reasons. First, as it is the aim of this paper to compare mechanical effects, it is necessary to justify that the previous mechanical history is erased during the melting phase. Second, by time-temperature superposition, the mobilities in the undercooled melt at T_c can be estimated, to evaluate the time scales of stress relaxation and the decay of flow-induced orientation. The relaxation time spectrum of the molten iPP was determined from the linear viscoelastic moduli (G′ and G″). The latter were measured using parallel plate geometries with a Rheometric Mechanical Spectrometer 800 and a Dynamic Stress rheometer (both from Rheometric Scientific, USA) at temperatures of 190, 210, 230, and 250 °C. Time-temperature superposition was used to obtain a master curve and the shift factor was determined, the data are shown in Fig. A of the supporting information. The activation energy was found to be 47 kJ/mol, which is typical for an isotactic polypropylene. A broad relaxation spectrum was observed. The longest relaxation time τ_0 is of special interest. It was determined from creep experiments, which were performed over a range of stresses from 1 to 100 Pa where the response was linear. For the linear viscoelastic case, τ_0 can be obtained by extrapolation from the regime of steady rate of straining $\dot{\gamma}_\infty$:

$$\tau_0 = \frac{\gamma_0}{\dot{\gamma}_\infty} \tag{5}$$

where γ_0 is the strain by extrapolating of the limiting slope to time zero. The longest relaxation time at a temperature of 210 °C estimated in this way is 7 s, which agrees with the value estimated from the spectrum. From the activation energy and the shift factors, the changes in the relaxation spectrum in the undercooled state, at the isothermal crystallization temperature used in this study (T_c = 136 °C), can be estimated. This estimate will be conservative, as in a crystallizing melt, mobilities are probably even slower as the polymer crystallizes. An estimate of the longest relaxation time at the crystallization temperature is of the order of 50 s.

The longest relaxation time in the molten state is shorter than the time the samples are kept in the melt at 210 °C, enabling a relaxation of effects occurring during loading of the samples. Athermal nuclei might still be present, as suggested by Alfonso and Ziabicki (1995). The strict protocol that was followed, however, keeps these effects constant and enables a systematic study of the effect of flow on the crystallization of polypropylene.

In the present work we want to investigate the regime where the morphological entities remain spherulitic. Acierno et al. (2003) showed that the transition to non-isotropic morphologies is controlled by a critical value of the Deborah number, defined as the longest relaxation time times the shear rate. This critical value was estimated to be 160 in the case of a polybutene. In our case aligned morphologies are clearly observed at a shear rate of 10 s^{-1} at 136 °C (corresponding to

De ∽ 500). An example of such an aligned structure is shown in Fig. B of the supporting information. In the following, we will restrict ourselves to shear rates below 2 s^{-1} (De ∽ 100), where the morphologies were observed to be essentially isotropic. An example of a typical micrograph at 2 s^{-1} is also included in Fig. B of the supporting information.

Linear birefringence

Orientation during flow was measured by flow birefringence. Figure 3 shows the evolution of the transient birefringence in the velocity gradient plane ($\Delta n'_{13}$), at different shear rates with the other flow parameters being fixed ($t_0 = 0$ s, $t_S = 30$ s). As can be expected, the plateau level of orientation and hence the overall stress level increases with increasing shear rate, and in the shear rate range explored obeys a power law:

$$\Delta\eta' \propto \dot{\gamma}^{0.83} \tag{6}$$

Describing the orientation relaxation after shear by an exponential decay results in a characteristic time of several seconds, which is in line with the estimation of the dominant relaxation time from the rheological measurements. Within experimental error, the birefringence relaxes to zero after cessation of shear flow. At longer times, the birefringence will start to increase again due to the appearance of crystalline entities, as studied in more detail by Liedauer et al. (1993) or Kumaraswamy et al. (1999). The reproducibility of the long time evolution in our experiments was, however, poor and it has not been further explored.

Experiments at fixed total strain and shear rate, where only the instant at which flow applied is varied, are shown in Fig 4. As expected, the orientation level at the end of the shear flow was the same, as long as t_0 is short. Only the instant in time at which the polymers become oriented is varied. In a last set of birefringence experiments, shown in Fig 5, the total strain is varied, but the instant in time at which flow is stopped ($t_0 + t_S$) and the shear rate ($\dot{\gamma} = 0.5$ s^{-1}) are fixed. As the shearing time (t_S) is increased, the birefringence first increases monotonically. Subsequently, it passes through a shallow maximum before reaching a steady level after

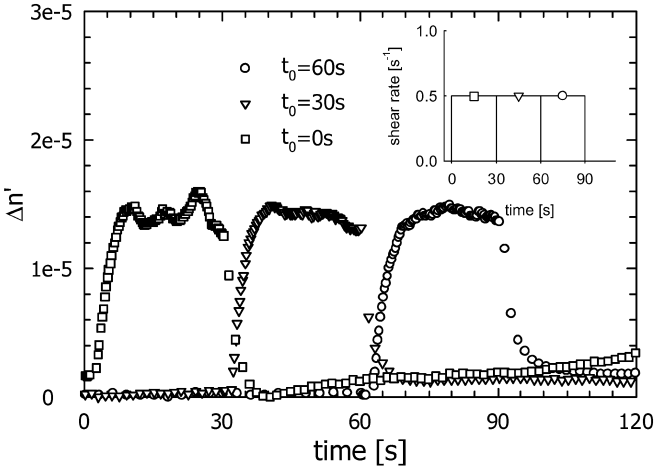

Fig. 4 Effect of instant of the start of shear flow on flow birefringence during transient shear flows at $T_c = 136$°C, $\dot{\gamma} = 0.5$ s^{-1}, $t_S = 30$ s, t_0 is varied, as schematically depicted in the *insert*

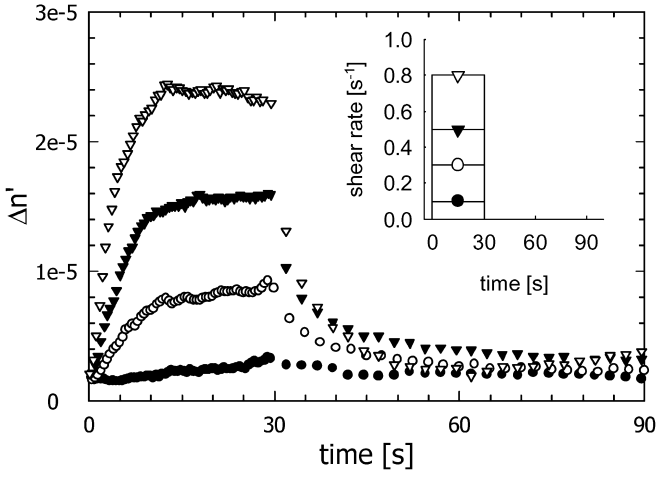

Fig. 3 Effect of the shear rate on the flow birefringence during a transient shear flow at Tc = 136 °C. Shearing time $t_S = 30$ s, shear rate is varied using 0.1 s^{-1} : *filled circles* 0.3 s^{-1}: *open circles*, 0.5 s^{-1}: *filled inverted triangles* and 0.8 s^{-1}: *open inverted triangles*, $t_0 = 0$, as schematically depicted in the *insert*

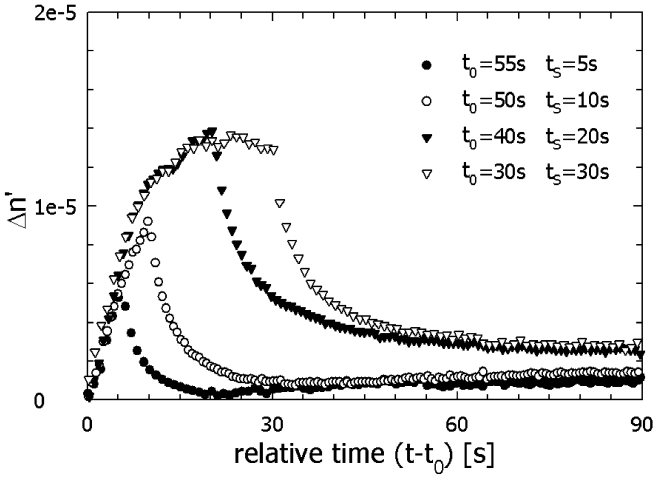

Fig. 5 Effect of the shearing time on flow birefringence in transient shear flow experiments at $T_c = 136$ °C, shear rate $\dot{\gamma} = 0.5$ s^{-1}, varying t_S, while keeping $t_0 + t_S = 60$ s. Note that the data are plotted as a function of the relative time since the inception of flow

roughly 30 s. Upon cessation of flow, the birefringence relaxes. As can be observed in Fig 5, for larger t_S values, the birefringence does not relax completely to zero. However, due to baseline drift and residual birefringence in the quartz plates of the Linkam shear cell this could be an experimental artifact. Most of the birefringence relaxes on times scales which agree with those expected from the rheological experiments.

Overall kinetics

In Fig 6, the evolution of α is plotted as a function of time for a series of preshear histories similar to those presented in Fig 3. In the absence of flow, α starts to increase only after 600 s, and crystallization is complete after about 5000 s, in agreement with the optical observations mentioned above. When a flow is applied immediately after reaching isothermal conditions for a duration t_S of 30 s, a shift of the DLI curves on the time axis is observed. As is shown in Fig 6, the sigmoidal curves are shifted parallel to each other on a linear-log scale. At the highest shear rate used here, the time to reach complete crystallization has been reduced by an order of magnitude. To quantify the acceleration of kinetics, we use an Avrami analysis (Avrami 1940) for the overall kinetics. The following well-known expression for the overall kinetics of isothermal crystallization:

$$\ln\left(-\ln\left(1-\alpha(t)\right)\right) = \ln k + n\ln\left(t\right) \tag{7}$$

was fitted to our data. The Avrami coefficient n is found to be 2.5 ± 0.1 for quiescent crystallization at 136 °C for α between 0.05 and 0.6. In this range of α, the value of n remains unchanged for the shear-induced crystallization experiments. This is consistent with the observation that morphologies remain essentially spherulitic in the range of strains explored. The value of $n = 2.5$ is rather small compared to theoretical predictions for spherulites which are between 3 and 4 depending on the nucleation mode, but similar values are often reported for instantaneous nucleation in polypropylene crystallization (Seo et al. 2000). Kinetics are characterized in terms of the rate constant k, while fixing the Avrami coefficient n to 3, which corresponds to the theoretical value for of instantaneous nucleation and 3D growth. Using the latter value renders a comparison with published work possible. Using a different numerical value of n does not fundamentally alter the results. The coefficient k can now be used to quantify the enhancement of the kinetics.

Figure 7 shows the evolution of the ratio k_{shear}/k_{static} for the experiments of Fig 6. A power law behavior is obtained:

$$k_{shear} \propto \dot{\gamma}^{1.22} \tag{8}$$

The effect of total strain on the overall kinetics was analyzed in the same manner the data are added in Fig 7. At a shear rate of 0.4 s^{-1} and constant $t_0 + t_S$ the following power law is obtained from the Avrami analysis:

$$k_{shear} \propto t_S^{0.77} \tag{9}$$

We could not extend our measurements to larger strains, as shear fracture occurred.

Following the experimental protocol used for the birefringence experiments of Fig 4, the shear rate and

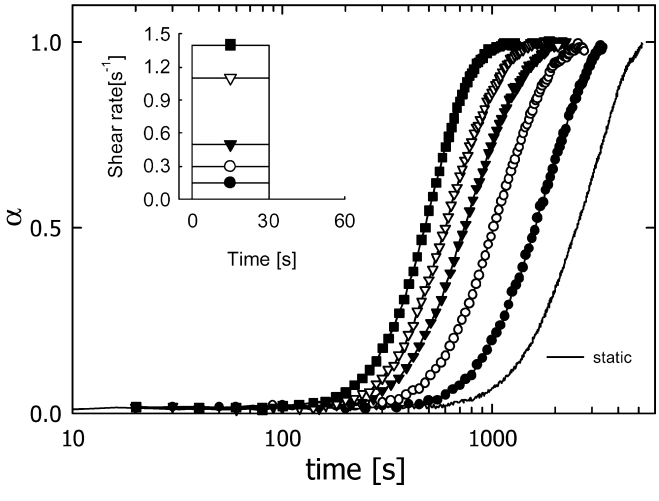

Fig. 6 Effect of the shear rate on the evolution of $\alpha(t)$ in quiescent conditions and for shear-enhanced crystallization at $T_c = 136°$ ($t_S = 30$ s, $t_0 = 0$, as schematically depicted in the *insert*), shear rates used were 0.15 s^{-1}: *filled circles* 0.3^{-1}: *open circles*, 0.5 s^{-1}: *filled inverted triangles*, 1 s^{-1}: *open inverted triangles* and 1.4 s^{-1}: *filled squares*

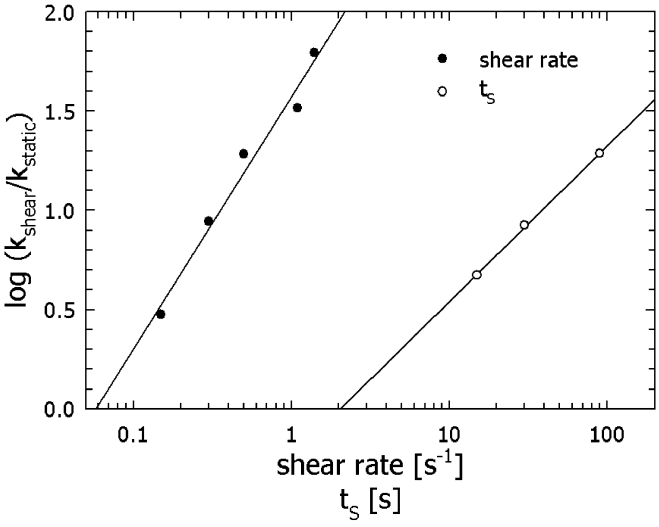

Fig. 7 Effect of the shear rate (at constant shearing time = 30 s and $t_0 = 0$) and shearing time (at constant shear rate 0.4 s^{-1}) and on the kinetic rate constant k_{shear}/k_{static} calculated from the DLI experiments

the time of shearing are kept constant in the next set of DLI experiments (Figs. 8 and 9), while the instant of application of flow t_0 is varied. Intuitively, one would expect that, as the sample is sheared earlier in time and nuclei would be created during flow, the subsequent crystallization would set in quicker. However, Fig 8 shows that the overall kinetics are not affected by the instant at which flow is applied over a wide range of dwell times. Figure 8 compares the evolution of the overall kinetics under static conditions with experiments at shear rates of 0.4 s^{-1} and 0.7 s^{-1} . For both shear rates, t_S was fixed at 30 s, whereas t_0 was varied between 0 and 300 s. Even though a log scale is used on the time axis, it should be noted that differences in t_0 of more than 200 s have been used, and instead of finding distinct parallel curves, shifted along the time-axis, all curves for a given shear rate and shearing time collapse. Hence a broad time window exists in which the waiting time t_0 does not affect the subsequent kinetics. The data in Fig 8 shows that, at shear rates of 0.4 s^{-1} and 0.7 s^{-1} and a shearing time of 30 s, this time window can extend to 100 s, exceeding the longest relaxation time of the polymer.

Nevertheless, a maximum dwell time ($t_{0,max}$) should exist. Indeed, increasing t_0 beyond a certain value, an effect on the kinetics is observed. Figure 9 shows α as a function of time for various t_0 at a shear of 1 s^{-1}, $t_S = 30$ s. Although under all conditions, an increase of the kinetics with respect to the static condition is still observed, waiting beyond a critical time, $t_{0,max}$, is observed to delay the onset of crystallization. Past this time, the slope of the sigmoid also changes, indicating a different evolution of crystallization. This maximal dwell time was observed to be a decreasing function of shear rate and shearing time.

SALS

Quiescent crystallization.

The evolution of density and orientation "fluctuations" in the melt at the crystallization temperature are detected by small-angle light scattering as used by Okada et al. (1992) and Winter and coworkers (Pogodina et al. 1999, 2001). The invariants Q_δ and Q_η during isothermal static crystallization at 136 °C are plotted as a function of time in Fig 10 together with the evolution of α. Density fluctuations (Q_η) are detected at the very early stages and a significant level is reached before orientation fluctuations (Q_δ) appear. The latter are related to spatial variations of the optical anisotropy due to the creation of crystals. The behavior of Q_δ tracks, albeit with a different sensitivity than α, the evolution of the fraction of crystalline material. The evolution of Q_η, in contrast, offers complementary information. Important variations in the optical density are shown to develop at first; subsequently during the crystalline growth phase the homogeneity of the melt increases again and Q_η will decrease. To evaluate the length scales at which these phenomena occur, the time evolution of the scattering intensities was also analyzed by a Debye-Bueche analysis

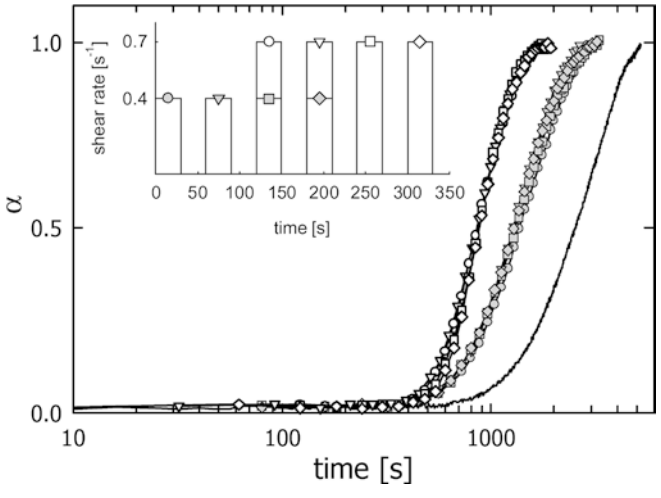

Fig. 8 Effect of the instant of the application of the shear on the evolution of $\alpha(t)$ for experiments with varying t_0, using fixed shear rates (0.4 and 0.7 s^{-1}) and a constant shearing time ($t_S = 30$ s), as compared to the quiescent conditions. For the shear rate of 0.4 s^{-1} (*gray symbols*), t_0 was varied from 0 s: *circles*, 60 s: *inverted triangles*, 120 s: *squares*, to 180 s: *diamonds*. For the shear rate of 0.7 s^{-1} (*open symbols*) t_0 was varied from 120 s: *circles*, 180 s: *inverted triangles*, 240 s: *squares*, to 300 s: *diamonds*

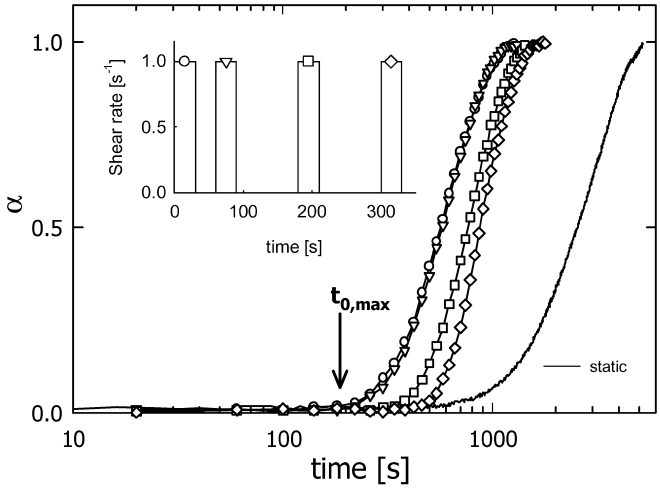

Fig. 9 Effect of the instant of the start of shear flow on the evolution of $\alpha(t)$ for experiments using a fixed shear rate of 1 s^{-1} and a constant shearing time of $t_S = 30$ s, as compared to the quiescent conditions. The "dwell time" t_0 was varied from 0: *open circles*, 60 s: *open inverted triangles*, 180 s: *open squares*, to 300 s: *open diamonds*. The critical point $t_{0,max}$ is shown by the *arrow*

(Debye and Bueche 1949). The correlation lengths of the density fluctuations and their evolution in time were probed. In agreement with the values reported by Pogodina et al. (1999), the size of the correlation was found to be of the order of 1 μm, of the same order as the wavelength. Microscopic observations where the number of nuclei at later times were counted, showed separation distances between nuclei much larger than the correlations lengths probed by the SALS experiments. This implies that only a fraction of the density fluctuations can be associated with the formation of a nucleus.

The effect of the crystallization temperature on the evolution of Q_η is shown in Fig 11 for temperatures ranging from 132 to 138 °C. All measurements were performed keeping the laser intensity constant; the invariants were referenced using the transmitted light intensity to a reference situation which was chosen to be static crystallization at 136 °C. Increasing the degree of undercooling affects both the relative importance of the density fluctuations and the kinetics of their development and disappearance: as the undercooling is increased, the maximum of Q_η shifts to shorter times and higher values (Fig 11).

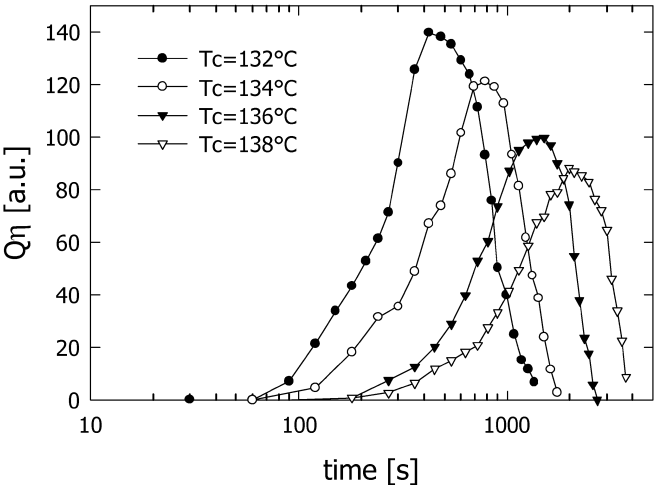

Fig. 11 Effect of temperature on the evolution of scattering invariants Q_η during quiescent crystallization at four different temperatures. The values of the scattering invariants were referenced to each other using the transmitted light intensity at scattering angle 0°

Shear-enhanced crystallization

The effect of preshearing on the evolution of the SALS patterns was investigated systematically. It was observed that, in the range of shear rates explored, the Vv patterns were essentially isotropic and 4-lobe H_v scattering patterns are obtained after crystallization. Therefore, the assumptions of the Stein-Wilson analysis remain valid, and the same analysis protocol as used for quiescent experiments was applied. Figure 12 shows the evolution of the scattering invariant Q_η for a range of shear rates corresponding to the data presented in Fig 3 and 6. Qualitatively, the effects of the mild flow conditions on the evolution of the SALS invariants are similar to the changes of temperature reported in Fig 11 (the same normalization procedure was used). Shearing enhances the fluctuations and speeds up their kinetics.

Figure 13 displays the evolution of the invariants Q_η and Q_δ for an experiment at a shear rate of 1 s^{-1} and

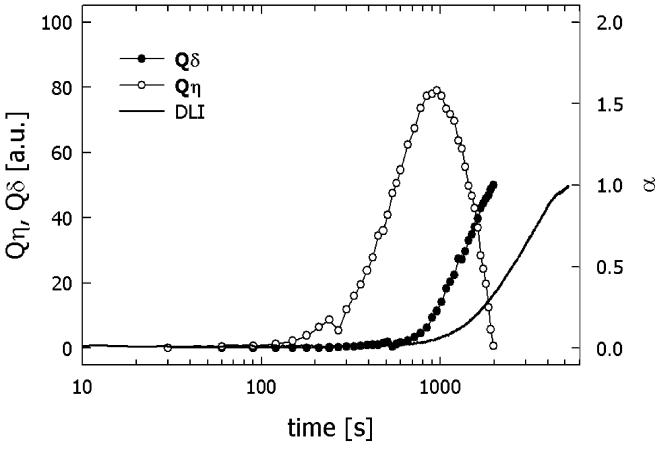

Fig. 10 Evolution of α and the scattering invariant Q_δ and Q_η at a temperature of 136 °C and quiescent conditions

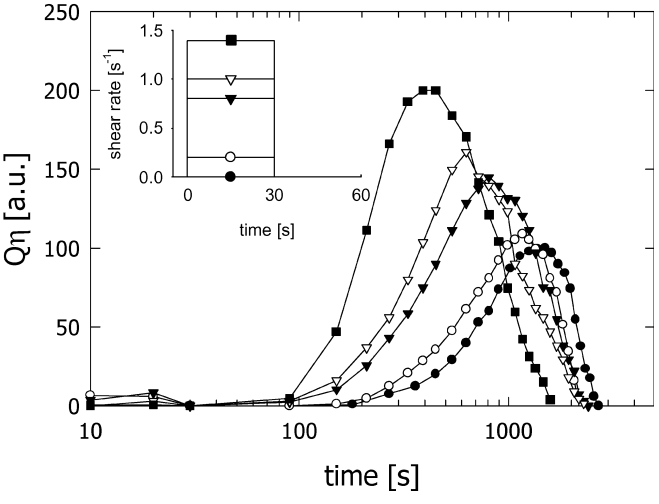

Fig. 12 Effect of the shear rate on the evolution of the scattering invariant Q_η at T = 136 °C for four different shear rates (0.2 s^{-1}: *open circles*, 0.8 s^{-1}: *filled inverted triangles*, 1 s^{-1}: *open inverted triangles*, 1.4 s^{-1}: *open squares*) while keeping the other parameters constant ($t_0 = 0$, $t_S = 30$) as compared to the static condition (*filled circles*). The values of the scattering invariants were referenced to each other using the transmitted light intensity at scattering angle 0°

$t_0 = 0$ s. For this sample, it was shown in Fig 9 that there was a critical time $t_{0,max}$ before which the waiting time had no effect. The time where the density invariant $Q\eta$ starts to increase corresponds quite well to the time $t_{0,max}$. This agreement between $t_{0,max}$ and the onset of measurable density fluctuations was also observed for shear rates of 0.4 and 0.7 s^{-1}.

Discussion

The effects of shear rate $\dot{\gamma}$ and shearing time t_S on the overall crystallization kinetics were evaluated quantitatively. Expressed in terms of the Avrami equation, using DLI experiments, the results have been summarized in Fig 7. By extrapolation of the data for shear rate in Fig 7, the value of a lower critical shear rate can be estimated to be 0.06 s^{-1} . This is on the order of the inverse of the longest relaxation time in the undercooled melt ($\tau_0 \backsim 50$ s). Above this shear rate a substantial enhancement of the kinetics is observed. Extrapolation of the data in Fig 7 for the shearing time also suggests the existence of a critical shearing time t_S min = 2 s for $\dot{\gamma} = 0.4$ s^{-1} . The dependence of the kinetic constants on shear rate and shear time displays power law behavior over the shear rates probed. Again, in agreement with previous works (Liedauer et al. 1993; Vleeshouwers and Meijer 1996), shear rate is a more effective parameter than shearing time. The Deborah numbers, based on the longest relaxation time, were larger than one. The shear rates in our experiments were, however, smaller than the inverse of the shortest relaxation time which could be probed in the linear oscillatory measurements, and the Rouse regime was not reached in the latter experiments (see Fig. A of the supporting information). It can be concluded that the shear rates in the present experiments were still below the regime where local chain extension would be strongly affected.

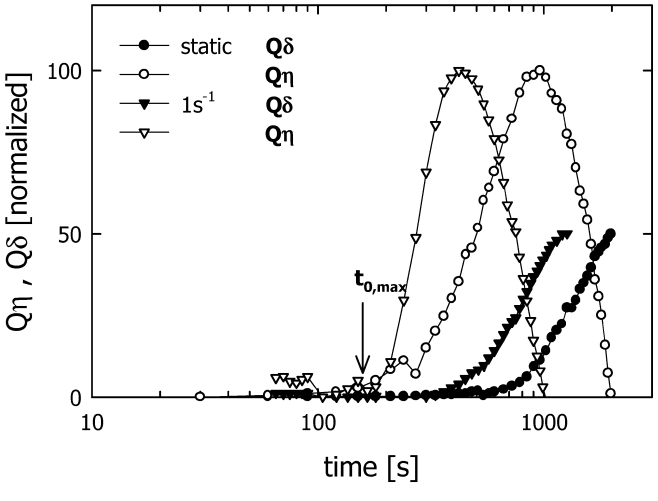

Fig. 13 Comparison of the time evolution of the scattering invariants with the characteristic dwell time $t_{0,max}$ as obtained from Fig. for a shear rate of 1 $s_{-1}$and the quiescent conditions. For the sake of clarity, all invariants have been normalized (Q_η to 100 a.u. and Q_δ to 50 a.u.)

Birefringence measurements were used to evaluate the effect of the orientation of macromolecules on the observed dependencies on shear rate and time. From a thermodynamic point of view, orientation reduces the entropy of the melt, which widens the degree of undercooling, and hence flow-enhanced crystallization has been explained by a simple modification of classical theories for quiescent crystallization (see, e.g., McHugh 1982; Coppola et al. 2001). In our experiments, the flow-induced orientation has almost completely relaxed when crystallization sets in, as can be seen by comparing Figs. 3 and 6. The crystallization kinetics shown in Fig 6 show that the crystallization only starts after an induction time between 200 and 800 s, when the flow-induced orientation has relaxed. Nevertheless, as Figs. 6 and 7 show, significant acceleration effects are observed.

The effect of shearing time (strain) was evaluated separately by varying the shearing time at constant shear rate while keeping the instant in time at which flow was stopped ($t_0 + t_S$) constant (see Figs. 5 and 7). The analysis of the crystallization kinetics shown in Fig 7 shows that the ratio k_{shear}/k_{static} keeps increasing with shearing time, much beyond the time needed for $\Delta n'$ to evolve past its maximum towards its plateau value. As can be seen in Fig 5, this time is on the order of 20 s at a shear rate of 0.5 s^{-1} , whereas Fig 7 shows that for shearing times up to 90 s at this shear rate no saturation of the enhancement seemed to occur. The effect of shearing time seems to indicate that the crystallization kinetics are sensitive to the cumulative effects of shear rate and shear time the material has experienced. It has, however, been reported recently that a saturation of the effect of t_S is eventually obtained (Kumaraswamy et al. 1999).

The most striking result in our experiments concerns the effect of the instant of application of the shear t_0 (or "dwell time"). Figure 8 shows that kinetics of crystallization are not affected by t_0 over a wide time window, as long as similar shear conditions (shear rate $\gamma\cdot$, time of shearing t_S) are used. It is known that the effect of flow is mainly to enhance the nucleation rate (Tribout et al. 1996). According to the classical view on the effects of flow, numerous nuclei could be activated by molecular orientation during the shear period.

These nuclei, formed during shear time t_S, add up to the thermally activated nuclei which occur spontaneously in the absence of flow. The thermal activation continues when the shear flow is stopped. According to the classical theory, no time-lag is needed between nucleation and crystalline growth, and hence the relevant timescale for the overall kinetics should be that

since the inception of shear. As a consequence, for the same γ·and t_S, when the dwell time t_0 is increased distinct crystallization curves should be observed as the nuclei should develop at different instants in time when the samples were sheared at different instants t_0. The independence with respect to, which is observed in the experiments presented in Fig 8, t_0 suggests, contrary to the previous interpretation, that nuclei activated by the thermomechanical history are not simply being formed during flow. In addition to the overall kinetics the evolution of the SALS invariants are also independent of t_0, as long as $t_0 \leq t_{0,max}$ (the latter are shown in Fig. C in the supporting information). The independence with respect to t_0 is an important result with respect to understanding of the effects of flow and the modeling of FIC.

When flow is delayed past a critical "dwell-time" $t_{0,max}$, the effect of t_0 becomes more in line with the behavior that would be expected intuitively. Waiting longer to apply a shear flow delays the onset of crystallization. The situation becomes, however, more complicated as flow, nucleation and growth phenomena interfere. Rather than observing a mere parallel shift of the conversion curves, the slopes of the sigmoids in Fig 9 start to change. Past the time $t_{0,max}$, the crystalline growth seems to begin during the period of shearing and shear-activated nucleation is not so efficient anymore.

The SALS experiments support the observations from the effects of flow on crystallization kinetics and provide a link between the time $t_{0,max}$ and the microstructural evolution. The quiescent crystallization experiments of, e.g., Fig 10 revealed the behavior already reported by Okada et al. (1992) and Pogodina et al. (1999). Density fluctuations were observed before orientation fluctuations start to develop. Pogodina et al. (1999) identified the increase in Q_η with the growth of low anisotropic structures of unknown origin which were shown to be on the order of 1 micrometer in size. Akpalu et al. (1999) have shown using X-ray scattering that locally more dense zones exists, possibly oriented but not necessarily crystalline zones, which contain the precursors of nuclei. The fact that Q_η reaches a maximum has to do with the fact that these clusters form a volume spanning network, which also affects the rheology (Pogodina et al. 1999). The invariant Q_η, which tracks the importance of the spatial variations in density, will hence be an indirect measure for the amount of nuclei that will be formed. Comparing evolution of the invariants in Fig 13 with the evolution of α in Fig 9 for a shear rate of 1 s^{-1} but different t_0 suggests that the maximum dwell time $t_{0,max}$ corresponds rather well to the time when the invariant density fluctuations start to become measurable. The same correspondence between $t_{0,max}$ and the onset of the evolution of Q_η was also obtained for two other shear rates (0.4 and 0.7 s^{-1}). The data in Fig 9 suggest that, as long as t_0 is smaller than $t_{0,max}$, only the intensity ($\dot{\gamma}$) and duration (t_S) of the flow affect the kinetics, although not when it has been applied. When delaying past this time $t_{0,max}$, density variations have pronouncedly developed as they become "visible" in the SALS experiments. Possibly coalescence of nuclei, a complex coupling between the variations in density and the shear flow or an increased growth rate during flow occur.

To evaluate the effects of flow in more detail, it is helpful to compare the evolution of the scattering invariants under quiescent conditions at different temperatures with the effects of flow at fixed temperature. Decreasing the temperature (see Fig 11), the same qualitative evolution of the invariants is observed, but the curves are shifted along the time axis. Comparing the evolution of Q_η with the well known effect of temperature on α (Pogodina et al. 1999; Devaux 2003) shows that the shift of time at which the maximum in Q_η occurs is similar to the characteristic time of the overall crystallization kinetics. Using the non-polarizing beamsplitter and a photodiode, a quantitative comparison of the relative magnitudes of the invariant was also made possible, showing an increase of the maximum of the invariants with increased undercooling.

The evolution of the invariants was also used to characterize the effects of the shear flow on the early stages of crystallization. The study of this effect was facilitated by the low anisotropies of the scattering patterns in the shear rate range explored. Whereas anisotropic birefringent structures develop at higher shear rates, the application of shear flow leads first and foremost to an earlier development of the density fluctuations as is shown in Fig 12. The effect of an increase in shear rate is qualitatively similar to a decrease in temperature. However, when the value of the maximum

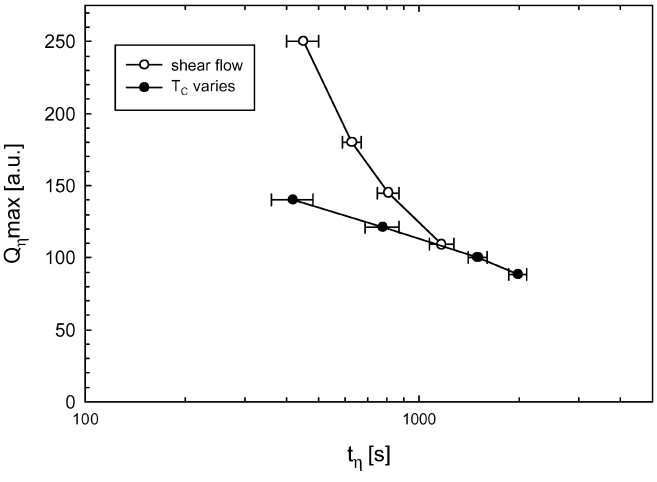

Fig. 14 Comparison of the effect of shear rate and temperature on the magnitude of the maximum of Q_η plotted vs the instant in time t_η at which this maximum is reached (data from Figs. 11 and 12)

in Q_η and the time t_η at which this maximum occurs are compared in Fig 14, it can be deduced that there are clear differences between temperature and flow effects. For a certain acceleration of the kinetics, as inferred from a reduction in t_η, density fluctuations need to develop to a larger extent for the case of flow-enhanced crystallization. As suggested by Pogodina et al. (1999), it has been shown that the early stages of evolving microstructure are the ones that flow affects predominantly.

Conclusions

The enhancement by a shear flow of the kinetics of isothermal crystallization of an isotactic polypropylene has been studied experimentally. The magnitude of the shear rate, the shearing time as well as the moment in time at which the deformation starts have all been varied and their effects have been quantified for the case of point like nuclei and spherulitic structures. The higher the shear rate and/or the larger the total strain, the more the kinetics are enhanced. However, an intriguing observation, not previously described, is that the instant in time at which a defined shear is applied was found to not affect the evolution of the overall kinetics, as long as the flow is applied before the beginning of the densification ($t_{0,max}$). Density fluctuations were observed in the early stages of crystalline structure formation during both quiescent and shear-enhanced isothermal crystallization. Clearly, flow enhancement does not imply a change in the mechanism of crystallization, or in the crystalline structures developed subsequently. Temperature and flow have qualitatively similar effects on the time evolution of the density and orientation fluctuations, at least in the range of conditions explored. For the same acceleration of the kinetics, a shear flow does require a more pronounced development of the spatial variations in density as detected by SALS as compared to the static crystallization at greater undercooling.

Acknowledgments N.D. gratefully thanks Atofina (Paris, France) for financial support during his PhD thesis. J.V. acknowledges the Fund for Scientific Research Belgium (F.W.O. Vlaanderen) for Grant KAN99 1.5.109.99. Dr. B. Ernst and Dr. F. Ravilly (ATOFINA) are thanked for stimulating discussions.

References

Acierno S, Palomba B, Winter HH, Grizzuti N (2003) Effect of molecular weight on the flow-induced crystallization of isotactic poly(1butene). Rheol Acta 42:243–250

Akpalu Y, Kielhorn L, Hsiao BS, Stein RS, Russell TP, van Egmond JW, Muthukumar M (1999) Structure development during crystallization of homogeneous copolymers of ethene and 1octene: time-resolved synchrotron X-ray and SALS measurements. Macromolecules 32:765–770

Alfonso GC, Ziabicki A (1995) Memory effects in isothermal crystallization. 2. Isotactic polypropylene. Colloid Polym Sci 273:317–323

Andersen PG, Carr SH (1978) Crystal nucleation in sheared polymer melts. Polym Eng Sci 18:215–221

Avrami M (1940) Kinetics of phase change II. Transformation-time relations for random distributions of nuclei. J Chem Phys 8:212–224

Bashir Z, Odell JA, Keller A (1986) Stiff and strong polyethylene with shish kebab morphology by continuous melt extrusion. J Mater Sci 21:3993–4002

Binsbergen FL (1973) Heterogeneous nucleation in crystallization of polyolefins. 3. Theory and mechanism. J Polym Sci Polym Phys Ed 11:117–135

Coppola S, Grizzuti N, Maffettone PL (2001) Microrheological modeling of flow-induced crystallization. Macromolecules 34:5030–5036

Debye P, Bueche AM (1949) Scattering by an inhomogenous solid. J Appl Phys 20:518–525

Devaux N (2003) Influence d'un cissaillement sur les premiers stades de la cristallisation du polypropylene. PhD Thesis, Ecole nationale supérieure des mines de Paris

Ding Z, Spruiell JE (1996) An experimental method for studying nonisothermal crystallization of polymers at very high cooling rates. J Polym Sci Part B Polym Phys 34:2783–2804

Duplay C, Monasse B, Haudin JM, Costa JL (1999) Shear-induced crystallization of polypropylene: influence of molecular structure. Polym Int 48:320–326

Duplay C, Monasse B, Haudin JM, Costa JL (2000) Shear-induced crystallization of polypropylene: Influence of molecular weight. J Mater Sci 35:6093–6103

Fuller GG (1995) Optical rheometry of complex fluids. Oxford University Press, Oxford

Fuller GG, Mikkelsen KJ (1989) Optical rheometry using a rotary polarization modulator. J Rheol 33:761

Jerschow P, Janeschitz-Kriegl H (1997) The role of long molecules and nucleating agents in shear induced crystallization of isotactic polypropylenes. Int Polym Proc 12:72–77

Keller A, Machin MJ (1967) Oriented crystallization in polymers. J Macromol Sci-Phys B1:41–49

Kumaraswamy G, Issaian AM, Kornfield JA (1999) Shear-enhanced crystallization in isotactic polypropylene. 1. Correspondence between in situ rheooptics and ex situ structure determination. Macromolecules 32:7537–7547

Kumaraswamy G, Kornfield JA, Yeh F, Hsiao BS (2002) Shear-enhanced crystallization in isotactic polypropylene. 3. Evidence for a kinetic pathway to nucleation Macromolecules 35:1762–1769

Lagasse RR, Maxwell B (1976) Experimental study of kinetics of polymer crystallization during flow. Polym Eng Sci 16:189–199

Lauritzen JI, Hoffman JD (1973) Extension of theory of growth of chain folded polymer crystals to large undercoolings. J Appl Phys 44:4340–4352

Lefebvre AA, Lee JH, Jeon HS, Balsara NP (1999) Initial stages of nucleation in phase separating polymer blends. J Chem Phys 111:6082–6099

Liedauer S, Eder G, Janeschitz-Kriegl H, Jerschow P, Geymeyer W, Ingolic E (1993) On the kinetics of shear induced crystallization in polypropylene. Int Polym Process 8:236–244

McHugh AJ (1982) Mechanisms of flow induced crystallization. Polym Eng Sci 22:15–26

McHugh AJ, Spevacek JA (1991) The kinetics of flow-induced crystallization from solution. J Polym Sci Part B Polym Phys 29:969–979

Monasse B (1995) Nucleation and anisotropic crystalline growth of polyethylene under shear. J Mater Sci 30:5002–5012

Monasse B, Haudin JM (1985) Growth transition and morphology change in polypropylene. Colloid Polym Sci 263:822–831

Okada T, Saito H, Inoue T (1992) Time resolved light-scattering studies on the early stages of crystallization in isotactic polypropylene. Macromolecules 25:1908–1911

Pogodina NV, Siddique SK, van Egmond JW, Winter HH (1999) Correlation of rheology and light scattering in isotactic polypropylene during early stages of crystallization. Macromolecules 32:1167–1174

Pogodina NV, Lavrenko VP, Srinivas S, Winter HH (2001) Rheology and structure of isotactic polypropylene near the gel point: quiescent and shear-induced crystallization. Polymer 42:9031–9043

Pratt CF, Hobbs SY (1976) Comparative study of crystallization rates by comparative study of crystallization rates by DSC and depolarization microscopy. Polymer 17:12–16

Seo Y, Kim J, Kim KU, Kim YC (2000) Study of the crystallization behaviors of polypropylene and maleic anhydride grafted polypropylene. Polymer 41:2639–2646

Sherwood CH, Price FP, Stein RS (1977) Effect of shear on crystallization kinetics of poly(ethylene oxide) and poly(epsilon-caprolactone) melts. J Polym Sci Polym Symp 63:77–94

Stein RS, Wilson PR (1962) Scattering of light by polymer films possessing correlated orientation functions. J Appl Phys 33:1914–1922

Terrill NJ, Fairclough PA, Towns-Andrews E, Komanshek BU, Young RJ, Ryan AJ (1998) Density fluctuations: the nucleation event in isotactic polypropylene crystallization. Polymer 39:2381–2385

Tribout C, Monasse B, Haudin JM (1996) Experimental study of shear-induced crystallization of an impact polypropylene copolymer. Colloid Polym Sci 274:197–208

Vleeshouwers S, Meijer HEH (1996) A rheological study of shear induced crystallization. Rheol Acta 35:391–399

Wang ZG, Hsiao BS, Sirota EB, Srinivas S (2000) A simultaneous small- and wide-angle X-ray scattering study of the early stages of melt crystallization in polyethylene. Polymer 41:8825–8832

Wunderlich B (1980) Macromolecular physics, vol 2. Academic Press, New York